Nanoscale

Accepted Manuscript

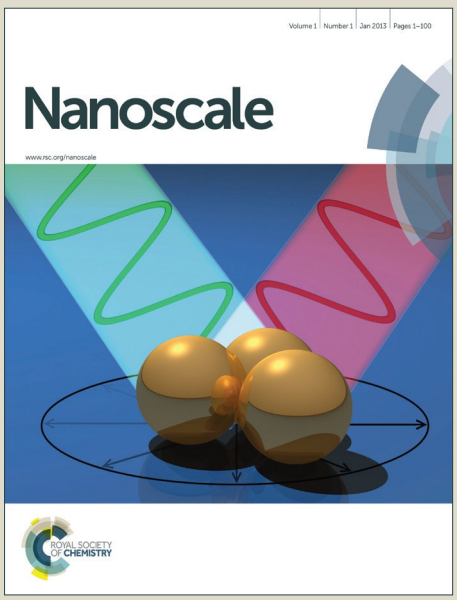

ROYAL SOCIETY OF CHEMISTRY

www.rsc.org/nanoscale

Journal Name

ARTICLE

Photonic crystal hydrogel suspension array for the capture of blood cells from whole blood

Received 00th January 20xx,
Accepted 00th January 20xx

DOI: 10.1039/x0xx00000x

www.rsc.org/

Bin Zhang, [‡a] Yunlang Cai,[‡b] Luoran Shang, [a] Huan Wang, [a] Yao Cheng, [a] Fei Rong, [ac] Zhongze Gu *[ac] and Yuanjin Zhao *[ac]

Diagnosing hematological disorders based on the separation and detection of cells in the patient's blood is a significant challenge. We have developed a novel barcode particle-based suspension array that can simultaneously capture and detect multiple types of blood cells. The barcode particles are polyacrylamide (PAAm) hydrogel inverse opal microcarriers with characteristic reflection peak codes that remain stable during cell capture on their surfaces. The hydrophilic PAAm hydrogel scaffolds of the barcode particles can entrap various plasma proteins to capture different cells in the blood, with little damage to captured cells.

Introduction

With the development of modern industry, the morbidity rate of hematological disorders has tended to increase in recent years. These hematological disorders have obscure symptoms and are easy to misdiagnose. [1-2] As a basic step in evaluating the functions of living cells and detecting disordered cells in bodily fluids, cell capture is particularly useful for dysfunctional platelet detection, immune cell analysis, and cancer diagnosis. Current strategies for cell capture based on microstructures, trapping arrays, or microfiltering microfluidic technologies, have offered many advantages in the analysis of cells. [3-6] However, these approaches usually perform simple cell capture, and cannot distinguish different blood cells, which is the key issue for the diagnosis of some hematological disorders. Therefore, constructing a platform that allows capture of multiple cell types is highly desirable, and it will pave the way to using blood cells in diagnostic and prognostic systems.

Suspension arrays, which use barcode particles as elements, have attracted increasing interest for multiple bioassays. [7-10] Many kinds of barcode particles, including fluorescent molecules, quantum dots, photonic crystals incorporated in microspheres, or graphical or shape-encoded microplates, have been proposed for suspension arrays. [11-22] Based on these barcode particles, many distinct suspension arrays have been created for multiple biomolecule detection, gene function analysis, and clinical diagnosis. However, the encoded information of most barcode particles may be incomprehensible when their surfaces are covered by cells, and this could cause false detection results. In addition, the debatable specificity and reliability of their general surface morphology and biochemical modification have also limited the application of barcode particles in the capture and detection of multiple types of blood cells. Thus, the development of novel barcode particle-based suspension arrays with distinct advantages is still required.

In this paper, we present a new type of suspension array that can simultaneously capture and detect multiple types of blood cells. The barcode particles of our suspension array are polyacrylamide (PAAm) hydrogel inverse opal microcarriers that are negatively replicated from spherical colloidal crystal templates. [23-27] The code of the microcarriers is the characteristic reflection peak originating from the stop-band of the inverse opal.[28-31] Because the peak position is based on their periodic structure, the code of the microcarriers is very stable and remains constant during cell capture and culture on their surfaces. In addition, the biocompatible hydrogel component and the ordered nanopore structure on the spherical surface of the barcode particles can provide not only more surface area for probe immobilization, but also a nanopatterned platform for highly efficient bioreactions of the probes and the surface proteins of the cells. Moreover, the hydrophilic PAAm hydrogel scaffolds of the barcode particles can entrap various plasma proteins to capture multiple cells in the blood, with little damage to the captured cells.[32, 33] These features make the barcode particles ideal for capturing and detecting multiple blood cells for the diagnosis and prognosis of hematological disorders.

[a] State Key Laboratory of Bioelectronics, School of Biological Science and Medical Engineering, Southeast University, Nanjing 210096, China.
E-mail: yjzhao@seu.edu.cn; gu@seu.edu.cn
[b] Department of Obestetrics and Gynecology, Zhongda Hospital, Southeast University,Nanjing 210009, China.
[c] Suzhou Key Laboratory of Environment and Biosafety, Research Institute of Southeast University in Suzhou, Suzhou 215123, China.
† Footnotes relating to the title and/or authors should appear here.
Electronic Supplementary Information (ESI) available: [details of any supplementary information available should be included here]. See DOI: 10.1039/x0xx00000x
‡ These authors contributed equally.

Results and discussion

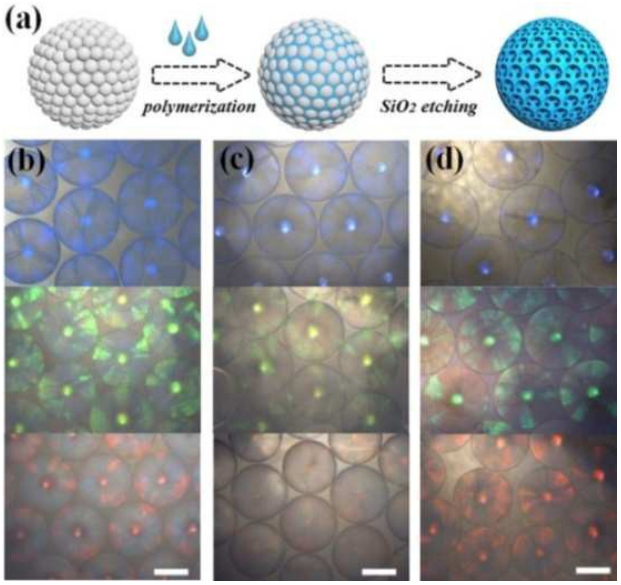

Figure 1.(a) Schematic illustration of the fabrication of the hydrogel inverse opal microcarriers. (b-d) The optical images of three kinds of microcarriers with different reflection peaks: (b) template colloidal crystal beads consisted of different size of silica nanoparticles; (c) hybrid colloidal crystal beads with PAAm hydrogel infiltration; (d) PAAm hydrogel inverse opal microcarriers that can directly employed for various plasma protein adsorption. Scale bars are 200 μm.

In a typical experiment, the hydrogel inverse opal microcarriers were fabricated by replicating spherical silica colloidal crystal cluster templates, as indicated in **Figure 1a**. These colloidal crystal cluster templates with high monodispersity were prepared by the self-assembly of silica nanoparticles in droplets, which became closely packed and formed an ordered structure in the beads during the evaporation of water. This ordered packing of the nanoparticles not only endows the spherical clusters with brilliant structural colors and reflection spectra (**Figure 1b** and **Figure S1**), but also forms connected nanochannels throughout the templates for infiltration of the pregel solution. To replicate the structure of the colloidal crystal clusters, the hydrophilically modified templates were first immersed in the pregel solution. After the pregel solution had penetrated the voids between the nanoparticles of the templates by capillary force, the mixture was exposed to ultraviolet light to polymerize the pregel solution in and out of the templates. Then, the prepared hydrogel containing the template particles was immersed in a buffer solution. During this treatment, the hydrogel exhibited obvious swelling. However, the silica nanoparticles were sintered and thus it was difficult for the hydrogel in the void spaces of the nanoparticles to swell consistently with the outer hydrogel because of the fixed template space. This difference in hydrogel swelling in and out of the templates caused hydrogel rupture on the surface of the colloidal crystal clusters. Thus, when the hydrogel was mechanically disrupted, the hybrid particles at the site of the rupture could fall off and be separated (**Figure 1c**). Finally, the hydrogel inverse opal microcarriers were obtained after removing the silica nanoparticles in the templates (**Figure 1d**).

To enable the entrapping of various plasma proteins on the surface of the microcarriers, the hydrophilic PAAm hydrogel, which is well known for its performance as both hydrogen bond donor and acceptor, was used as the scaffold material for the inverse opal structure. Thus, the pregel solution consisted of acrylamide (AAm) monomer, N,N-methylenebisacrylamide cross-linking, and 2-hydroxy-2-methylpropiophenone photoinitiator. In general, entrapping plasma proteins is enhanced by using a hydrogel with a large grid, which can be realized by reducing the concentration of pregel solution or decreasing the proportion of cross-linkers. In our experiment, we first fabricated inverse opal microcarriers by using a pregel solution with a concentration of 15% and a molar ratio of 30:1 for the monomer and the cross-linkers. We found that these fabricated microcarriers exhibited poor mechanical properties and strong adhesion to the centrifuge tube, which is unfavorable for the subsequent processes of protein adsorption and cell capture. After increasing the concentration to 30% and decreasing the molar ratio of the monomer and the cross-linkers to 10:1, the resultant PAAm hydrogel inverse opal microcarriers exhibited strong mechanical properties, reduced adhesion, and obvious structural colors, as shown in **Figure 1d**. Therefore, this concentration of the pregel solution was used to fabricate all the hydrogel barcode particles for the following experiments.

The microstructures of the spherical silica colloidal crystal cluster templates and the PAAm hydrogel inverse opal microcarriers were observed with a scanning electron microscope (SEM). **Figure 2** shows that the silica nanoparticles on the surface of the templates formed a hexagonal alignment (**Figure 2a**), and this structure extended inside the templates (**Figure 2b**). Thus, the PAAm hydrogel microcarriers replicated from the templates should have a similar highly ordered three-dimensional (3D) inverse opal structure. However, the hydrogel used for the fabrication of the PAAm inverse opal microcarriers was made with relatively low concentrations, and tended to shrink and collapse during the drying process (**Figure 2c**). To improve the effect of this replicate, a high concentration of ethylene glycol dimethacrylate cross-linker was employed to maintain the hydrogel scaffolds during drying. It can be observed that the microcarriers had an interconnected and hexagonal symmetrical porous surface (**Figure 2d**), which provided a nanopatterned platform for highly efficient entrapping of plasma proteins.

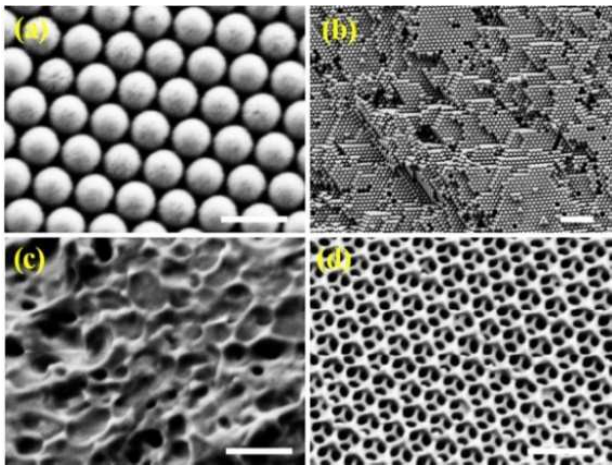

Figure 2.SEM images: (a, b) surface and inner structure of the colloidal crystal beads, which indicated commendable hexagonal close packing structure; (c) inverse opal microcarrier with collapse surface fabricated by lower concentration of the hydrogel ; (d) inverse opal microcarrier with interconnected porous surface by employing a high concentration of ethylene glycol dimethacrylate cross-linker. Scale bars are 400nm, 2um, 400nm and 400nm.

To investigate the plasma protein-entrapping capability of the PAAm hydrogel inverse opal microcarriers, solutions of fluorescein isothiocyanate-labeled fibronectin (FITC-FN) and fluorescein isothiocyanate-labeled phytohemagglutinin (FITC-PHA) were selected to incubate the microcarriers. Fluorescent images of the microcarriers in different concentrations of FITC-PHA protein are shown in **Figure S2**. We found that the microcarriers exhibited homogeneous green fluorescence, confirming that FITC-PHA was selectively entrapped on the microcarriers. In addition, the fluorescence density increased as the concentration of the protein increased, as shown in **Figure S3**. Also during the whole process of preserve, the fluorescent intensities of the protein enriched hydrogel particles at different times only exhibited slight changes (in the PBS buffer solution), which proved that the plasma proteins are irreversibly entrapped in the hydrogel particles. The high capacity of the PAAm microcarriers to entrap proteins should be ascribed to the hydrogen bond formation between the PAAm scaffolds and the plasma proteins. Furthermore, the 3D ordered and interconnected nanopores of the inverse opal PAAm scaffolds should also offer more contact sites for protein entrapping.

As fibronectin (FN) is a multifunctional plasma protein that can bind glycoproteins on the surface of the platelet membrane and phytohemagglutinin (PHA) is a glycoprotein that can agglutinate all human erythrocytes by ligand–cell reactions, the FN- or PHA-entrapped PAAm hydrogel inverse opal microcarriers gained the ability to capture specific blood cells (**Figure 3a**). To confirm this, the PHA-entrapped microcarriers were incubated in a concentrated suspension of erythrocytes and observed under SEM after the cell capture reaction. **Figure 3b–d** shows that most erythrocytes were specifically captured on the surface of the inverse opal microcarriers. The unique biconcave discoidal morphology of erythrocytes could be observed clearly in the SEM images (**Figure 3d**), confirming that the erythrocytes maintained their normal morphology and functionality. Similarly, the FN-entrapped microcarriers captured round morphology platelets on their surfaces (**Figure 3e–g**). These results indicate that specific blood cell capture can be achieved with little damage.

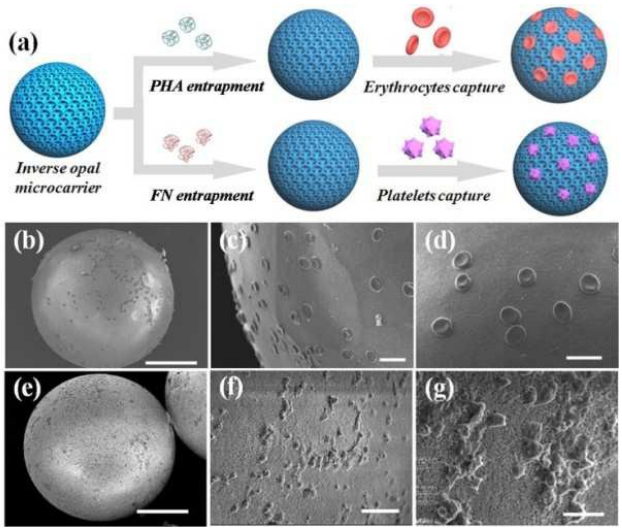

Figure 3.(a) Schematic illustration of blood cell capture by the hydrogel inverse opal microcarriers. (b-d) SEM images of captured erythrocytes on the surface of the PHA pre-adsorbed hydrogel inverse opal microcarriers. (e-g) SEM images of captured platelets on the surface of the FN pre-adsorbed hydrogel inverse opal microcarriers. Scale bars in (b)-(g) are 100um,10um,10um, 100um, 10um and 5um, respectively.

To achieve a high capture efficiency of blood cells on the PAAm hydrogel inverse opal microcarriers, we optimized the concentrations of the entrapped protein probes and the incubation times during the cell capture. For this purpose, the PAAm hydrogel inverse opal microcarriers were incubated in different concentrations of the PHA solutions and then used for the erythrocyte capture for different reaction times. The statistical results of the captured erythrocytes on the surface of the inverse opal microcarriers are shown in **Figure 4** based on the SEM images. The cells were counted in unit area under magnifying SEM images. We found that almost no erythrocyte was captured on the surface of virgin hydrogel microcarriers, while the number of captured erythrocytes gradually increased with increasing PHA entrapment, indicating the strong ability of the protein-decorated surface to capture blood cells (**Figure 4a**). When the concentration of the PHA was increased to 0.5 mg/ml, the density of the captured cells on the surface of the PAAm hydrogel inverse opal microcarriers reached a

stable level. For the incubation times during the cell capture, the results indicated that the number of captured cells initially increased with incubation time, and reached a plateau at an incubation time of 150 minutes (**Figure 4b**). Thus, the inverse opal microcarriers with optimized conditions were used for the following research. In comparable with the hydrogel inverse opal microcarriers, the colloidal crystal particles could also be employed as the microcarriers for the cell capture in this work. However, they only exhibited relatively lower cell capture efficiency (**Figure S4**). The advantages of the hydrogel inverse opal microcarriers should ascribe to the synergistic effects of the biocompatible hydrogel component and the ordered nanopore structure on their spherical surface.

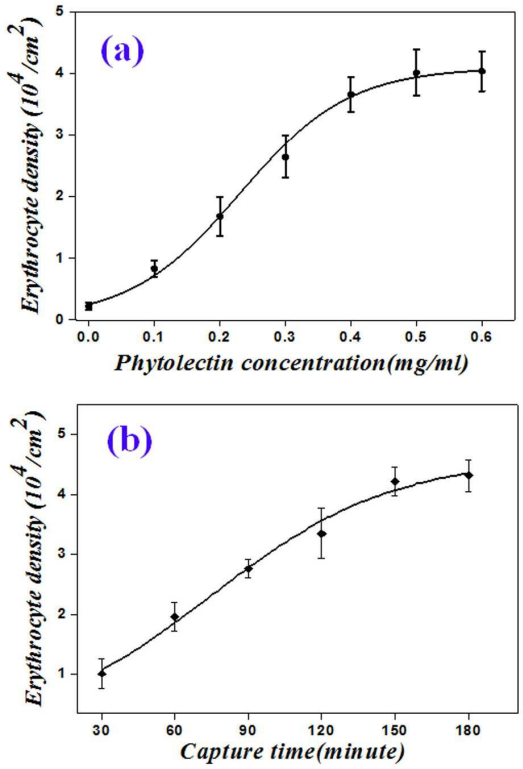

Figure 4.(a) The relationships of the cells number with the protein concentration. (b) The relationships of the cells number with the capture time. Error bars represent standard deviations.

when cells are captured on their surface (**Figure S5**). Both of these would cause mistakes when reading the encoded information of the barcode particles, and thus result in incorrect multiplexing results. In this research, we overcame this restriction by employing the characteristic reflection peak positions of the PAAm hydrogel inverse opal microcarriers as their encoded elements. When blood cells were captured on the microcarriers, they only interacted with the surface protein and could not destroy the periodic structure of the whole particle. As **Figure S6** illustrated, by adjusting the focal length of the microscope, the structural colors of the microcarriers with captured erythrocytes on their surface could still be observed. Also the reflection positions of the inverse opal particles with entrapped cells on their surface could still be detected. Since the hydrogel would shrink or swelling in different conditions, thus, in our research, we adopt a relative stable hydrogel for the research. The conditions were kept constantly during the whole cell capture process. As **Figure S7** showed, during the whole cell capture process, the change of reflection peak of the microcarrier was less than 10nm (indicated as R±5nm, R is the average peak position). Thus, to avoid the confusion of these changes, we can choose different barcode particles with the difference value of their reflection peak positions larger than 20nm.

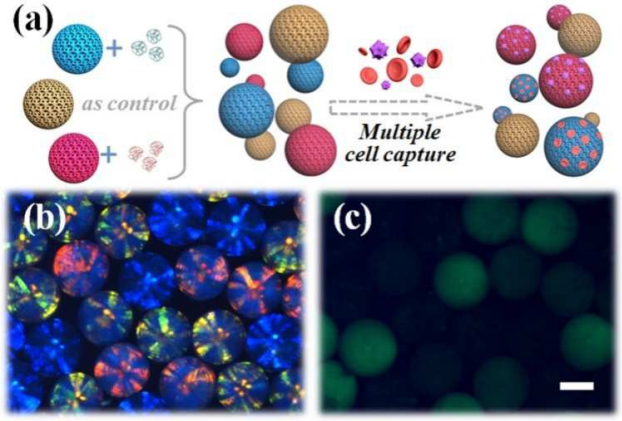

Figure 5.(a) Scheme diagram of the encoded microcarriers capturing multiple types of blood cells. (b, c) Optical microscopy and fluorescent image of three kinds of encoded microcarriers with characteristic reflection peaks at 660, 560, and 490 nm, which entrappted FITC-FN and FITC-PHA proteins labeled cells. Scale bar is 200um.

When using the barcode particles to capture multiple types of blood cells, an important challenge is the accurate identification of the encoded information during the entire reaction process. In general, barcode particles with fluorescent dyes or quantum dots (QDs) as encoded elements are limited in this application. Taking the QD particles for examples, their encoded fluorescent spectrum intensity could be decreased because of the coverage of the cell layer, or be affected by cell staining because of optical interference

To demonstrate the capability of the encoded PAAm hydrogel inverse opal microcarriers for capturing multiple types of blood cells in whole blood, three kinds of encoded microcarriers with characteristic reflection peaks at 660, 560, and 490 nm (hereinafter referred to as red, orange, and blue microcarriers, respectively) were employed, as shown in **Figure 5**. In this system, the red and blue microcarriers were entrapped with FN and PHA, respectively,

while the orange microcarriers served as a control with no protein adsorption. These microcarriers were then mixed and incubated in human whole blood. Because of the specific binding between the proteins and corresponding target blood cells, we expected to observe that different cells were captured on the surface of different kinds of inverse opal microcarriers. The results were first observed by SEM in **Figure S8**. Erythrocytes and platelets could be distinguished by their different morphology, which could be observed under magnifying SEM images. We found that platelets were mainly enriched on the red microcarriers, while erythrocytes were mainly enriched on the blue microcarriers, whereas the control group of orange microcarriers showed no obvious cell capture. And for a given type of sphere, their non-specific cells were less than 2%. These results were consistent with the content of the samples to which the encoded inverse opal microcarriers were exposed. Also we have employed flow cytometer to statistically analyze the blood cells before and after the capture, which confirm the multiple capture capability of our microcarriers (**Figure S9**). As hydrophilic PAAm scaffolds can entrap various plasma proteins with minimal damage to the captured cells, the PAAm hydrogel inverse opal microcarriers constructed here offer a new way to capture specific cells in the blood for disease diagnosis and therapy.

Experimental

Materials. Nine kinds of SiO_2 nanoparticles with the size of 200, 212, 238, 243, 252, 263, 275, 285 and 295 nm were purchased from NanJingDongJian Biological Technology Co., Ltd. Acrylamide (99.9%) and ethyleneglycol dimethacrylate was purchased from Alfa Aesar China Ltd (Heysham, Lancs). N,N'-methylenebisacrylamide cross-linking and 2-hydroxy-2-methylpropiophenone photoinitiator were purchased from Sigma-Aldrich (St. Louis, MO, USA) and used as received. Hydrofluoric acid, heparin sodium, glutaraldehyde and Phytohemagglutinin (PHA) were purchased from Aladdin Industrial Corporation (Shanghai, China). Fibronectin (FN) was purchased from Beijing Solarbio Science & Technology Co., Ltd. (Beijing, China). Fluorescein isothiocyanate-labeled fibronectin (FITC-FN) and Fluorescein isothiocyanate-labeled phytohemagglutinin (FITC-PHA) were purchased from Beijing biosynthesis biotechnology (China). Phosphate buffered saline (PBS, 0.1 mol/L, pH 7.4) and isotonic saline (NaCl solution, pH 7.4) were freshly prepared. All other reagents were of the best grade available and used as received.

30 healthy human blood samples were collected from the affiliated ZhongDa Hospital of Southeast University, Nanjing, China. All the collection and processing of human blood samples were carried out in accordance with the guidelines issued by the Ethical Committee of the Chinese Academy of Sciences.

Generation of template colloidal crystal cluster. The silica colloidal crystal cluster (SCCC) were prepared by the droplet template method. The aqueous suspension and silicon oil were injected into the microfluidic device. In consequence, the aqueous suspension was sheared into droplets by the oil flows in the microfluidic channel. The droplets were collected in a container filled with silicon oil. The silica nanoparticles self-assembled into ordered lattices during the evaporation of water in the droplets at 75°C in an oven. After solidification overnight, the silica colloidal crystal cluster were gently and thoroughly washed with hexane to remove the silicon oil. Finally, the silica colloidal crystal cluster were calcined at 800°C for 3h to improve their mechanical strength. The concentration of the used silica nanoparticles was 20% (w/v). The injection speeds of the oil and dispersed phase were 0.6mL/h and 8mL/h, respectively. Photographs of the SCCC were taken with a light microscope (OLYMPUS BX51) equipped with a color CCD camera (Media CyberneticsEvolutionMP 5.0). Reflection spectra of the SCCC were recorded by the microscope (OLYMPUS BX51) equipped with a fiber optic spectrometer (Ocean Optics, QE65000). The microstructures of the beads were characterized by a scanning electron microscopy (S-3000N, Hitachi, Japan) after freeze-dried and gold sputter coating.

Fabrication of hydrogel inverse opal microcarriers. The pre-gel solution used for the inverse opal microcarriers fabrication was composed of acrylamide, N,N'-methylenebisacrylamide and 2-hydroxy-2-methylpropiophenone (1% v/v). The mass ratio of acrylamide and N,N'-methylenebisacrylamide was 10:1. The inverse opal microcarriers were replicated from the voids of the template SCCC. To ensure the pre-gel solution could fill the void entirely, the SCCC were previously treated with piranha solution (30% v/v hydrogen peroxide and 70% v/v sulfuric acid) for 6h. After washing with water and drying by nitrogen flow, the SCCC were immersed in the pre-gel solution for 2h. They were then dispersed between two quartz disks separated by a 300-mm-thick spacer, and exposed to UV light (365 nm, 100 W, 10 minutes) for the polymerization of the pre-gel solution in and out of the SCCC. Broad-band excitation in the near-UV range (330–385 nm) was provided by a 100W mercury lamp. The prepared film containing the SCCC was immersed in the buffer solution for 1h in succession. After stirring the hydrogel film into pieces by a stirrer, the hybrid beads were filtered from the buffer solution. Finally, the inverse opal microcarriers were obtained after removing the silica template by immersed in hydrofluoric acid (4%, v/v) for 2h. Photographs, reflection spectra and microstructure pictures of the inverse opal microcarriers were measured as previously mentioned.

Entrapment of targeted proteins on the hydrogel inverse opal microcarriers. FITC-FN and FITC-PHA were dissolved in PBS at the concentrations from 0.1 to 0.8 mg/mL and the PAAm hydrogel inverse opal microcarriers were incubated in the prepared protein solutions for 60 min at 37 °C in the dark. Following the incubation, protein solutions were removed and the samples were gently washed twice with pre-warmed PBS (37°C). Then the fluorescence pictures of the microcarriers were taken by the microscope (OLYMPUS BX53) with a high resolution CCD (OLYMPUS DP73) and were processed by Cell Standard software to characterize the fluorescencein tensity through the obtained green grey value. The adsorption of FN and PHA without fluorescence labeling on patterned surface was performed according to procedure described above. And the FN-adsorbed and PHA-adsorbed patterned hydrogel inverse opal microcarriers were used to capture platelets and erythrocytes respectively.

Erythrocytes capture and cell counting. The citrated whole blood sample was centrifuged at 1000 rpm for 10 min at 4°C to separate erythrocytes, white blood cells (WBCs), and platelet rich plasma (PRP). Then the plasma and buffy coat layers (PRP and WBCs) were carefully removed and discarded. Erythrocytes concentrates were washed three times with isotonic saline (0.9% w/v of aqueous NaCl

solution, pH 7.4). Afterward, the erythrocyte pellets were resuspended in normal saline to obtain an erythrocyte suspension solution. Subsequently, the PHA-adsorbed PAAm hydrogel inverse opal microcarriers were placed in contact with erythrocyte suspension and incubated for 120 min at 37°C under static conditions to provide enough time to capture erythrocytes. After the incubation, the samples were carefully rinsed twice with pre-warmed PBS, followed by immersing in 0.3 mL of 2.5% (v/v) glutaraldehyde in PBS for 10 h at 4°C to fix the captured erythrocytes. Finally, the samples were dehydrated with gradient ethanol gradually. The common concentration gradient of ethanol is from 20%, 40%, 60%, 80% to 100%, and each concentration of ethanol dehydrated the cell samples for over 20 min. The cell captured samples were imaged by scanning electron microscope (S-3000N, Hitachi, Japan) after gold sputter coating.

After cell capturing, we analyzed and calculated how many cells were captured on the substrate using cell-counting software by SEM images. The number of total cells captured was calculated by multiplying the average cell-surface density on the surface area of the microcarriers. The cell-surface density (x) is determined by the average diameter (d) of the microcarriers and average cell number (n) on the hemispheric of the microcarriers, respectively, according to the equation of $x= 2n/\pi d^2$. In order to make sure the numbers and morphology of the captured erythrocytes and platelets are the same before and after drying, we chose to partly remove the template SCCBs to avoid the collapse of the hydrogel inverse opal microcarriers.

Platelets capture. The citrated whole blood achieved from hospital was first centrifuged (1000 rpm, 5 min, 4°C) to obtain the upper precipitation, and then it was centrifuged (3000 rpm, 30 min, 4°C) to finally get the lower precipitation consisted of platelet rich plasma (PRP). After equilibration with heparin sodium solution (1mg/ml in PBS), the FN-adsorbed PAAM hydrogel inverse opal microcarriers were placed in contact with PRP and incubated for 120 min at 37°C under static conditions. Then PRP was removed and the samples were gently rinsed three times with PBS to remove none adhered platelets. Subsequently, captured platelets were fixed using 2.5% (v/v) glutaraldehyde in PBS for 10 h at 4°C. Finally, the samples were dehydrated with gradient ethanol gradually. The common concentration gradient of ethanol is from 20%, 40%, 60%, 80% to 100%, and each concentration of ethanol dehydrated the cell samples for over 20 min. The cell captured samples were imaged by scanning electron microscope (S-3000N, Hitachi, Japan) after gold sputter coating.

Cell Capture from Whole Blood. To validate the feasibility of applying hydrogel inverse opal microcarriers in capturing multiple types of blood cells in whole blood, three kinds of inverse opal microcarriers with the characteristic reflection peak at 660, 560, and 490 nm (hereinafter referred to as red, orange, and blue microcarriers, respectively) were used in the multiple cell capture experiment. For this purpose, the red microcarriers were incubated with FITC-FN, and the blue microcarriers were entrapped with FITC-PHA, while the orange microcarriers served as a control with no protein adsorption. These microcarriers were then mixed and incubated in directly gained whole blood samples for 120 min at 37°C under static conditions. Subsequently, captured cells were fixed using 2.5% (v/v) glutaraldehyde in PBS for 10 h at 4°C. Finally, the samples were dehydrated with gradient ethanol gradually. The common concentration gradient of ethanol is from 20%, 40%, 60%, 80% to 100%, and each concentration of ethanol dehydrated the cell samples for over 20 min. The cell captured samples were imaged by scanning electron microscope (S-3000N, Hitachi, Japan) after gold sputter coating.

Conclusions

In summary, we have developed a novel barcode particle-based suspension array that can simultaneously capture and detect multiple types of blood cells. The barcode particles are PAAm hydrogel inverse opal microcarriers fabricated by negatively replicating spherical colloidal crystal templates. As the codes of the microcarriers were the characteristic reflection peaks originating from their periodic structure, they were very stable and remained constant during cell capture and culture on their surfaces. The hydrophilic PAAm hydrogel scaffolds of the inverse opal microcarriers entrapped various plasma proteins to capture multiple cells in the blood with little damage to the captured cells. In addition, the ordered nanopore structure on the spherical surface of the inverse opal microcarriers could provide not only more surface area for probe immobilization, but also a nanopatterned platform for highly efficient cell capture. These features make the PAAm hydrogel inverse opal microcarriers ideal for capturing and detecting multiple blood cells during the diagnosis and prognosis of hematological disorders.

Acknowledgements

This work was supported by the National Science Foundation of China (Grant Nos. 21473029, 91227124 and 51522302), the NASF Foundation of China (Grant No. U1530260), the National Science Foundation of Jiangsu (Grant No. BK20140028), the Science and Technology Development Program of Suzhou (Grant No. ZXG2012021), the Research Fund for the Doctoral Program of Higher Education of China (20120092130006), and the Program for New Century Excellent Talents in University.

Notes and references

1 C. Neunert, W. Lim and M. Crowther, Blood, 2011, 117, 4190.
2 J. N. George, Haematologica, 2009, 94, 759.
3 F. Y. Zheng, Y. Cheng, J. Wang, J. Lu, B. Zhang, Y. J. Zhao and Z. Z. Gu, Adv. Mater. 2014, 26, 7333.
4 E. N. Charles, V. Anita, G. Thomas, E. K. Tia, J. F. Rbert and D. Jens, Biosens. Bioelectron. 2015, 68, 382.
5 J. Lu, F. Y. Zheng, Y. Cheng, H. B. Ding, Y. J. Zhao and Z. Z. Gu, Nanoscale, 2014, 6, 10650.
6 J. Lu, X. Zou, Z. Zhao, Z. D. Mu, Y. J. Zhao and Z. Z. Gu, ACS Appl. Mater. Interf. 2015, 7, 10091.
7 N. Liu, W. F. Liang, X. H. Ma, X. L. Li, B. A. Ning, C. N. Cheng, G. R. Ou, B. G. Wang, J. Zhang and Z. X. Gao, Biosens. Bioelectron., 2013, 47, 92.
8 B. F. Ye, H. B. Ding, Y. Cheng, H. C. Gu, Y. J. Zhao, Z. Y. Xie and Z. Z. Gu, Adv. Mater., 2014, 26, 3270.

9 M. A. Makiya, J. A. Herrick, P. Khoury, C. P. Prussin, T. B. Nutman and A. D. Klion, J. Immunological Method. 2014, 411, 11.
10 Y. He, Y. X. Zha, M. Q. Zhu, Q. Y. Wu and C. G. Ruan, Clin. Chim. Acta 2013, 415, 176.
11 Y. J. Zhao, Y. Cheng, L. R. Shang, J. Wang, Z. Y. Xie and Z. Z. Gu, Small. 2015, 11, 151.
12 Z. W. Mao, H. L. Xu and D. Y. Wang, Adv. Funct. Mater., 2010, 20, 1053.
13 M. A. Al-Ameen, J. Li, D. G. Beer and G. Ghosh, Analyst, 2015, 140, 4530.
14 H. K. Yu, Z. W. Mao and D. Y. Wang, J. Am. Chem. Soc., 2009, 131, 6366.
15 S. H. Kim, J. G. Park, T. M. Choi, V. N. Manoharan and D. A. Weitz, Nature Commun., 2014, 5, 3068.
16 S. S. Lee, B. Kim, S. K. Kim, J. C. Won, Y. H. Kim and S. H. Kim, Adv. Mater., 2015, 4, 627.
17 J. P. Ge, Y. X. Hu and Y. D. Yin, Angew. Chem. Int. Ed., 2007, 46, 7428.
18 J. P. Ge and Y. D. Yin, Angew. Chem. Int. Ed., 2011, 50, 1492.
19 Y. J. Zhao, L. R. Shang, Y. Cheng and Z. Z. Gu, Acc. Chem. Res. 2014, 47, 3632.
20 L. R. Shang, F. Q. Shangguan, Y. Cheng, J. Lu, Z. Y. Xie, Y. J. Zhao and Z. Z. Gu, Nanoscale. 2013, 5, 9553.
21 J. Hou, H. C. Zhang, Q. Yang, M. Z. Li, Y. L. Song and L. Jiang, Angew. Chem. Int. Ed., 2014, 53, 5791.
22 W. Liu, L. R. Shang, F. Y. Zheng, J. L. Qian, J. Lu, Y. J. Zhao and Z. Z. Gu, Small, 2014, 10, 88.
23 T. Kanai, D. Lee, H. C. Shum and D. A. Weitz, Small, 2010, 6, 7807.
24 T. Kanai, D. Lee, H. C. Shum, R. K. Shah and D. A. Weitz, Adv. Mater., 2010, 22, 4998.
25 E. T. Tian, J. X. Wang, Y. M. Zheng, Y. L. Song, L. Jiang and D. B. Zhu, J. Mater. Chem., 2008, 18, 1116.
26 B. Zhang, Y. Cheng, H. Wang, B. F. Ye, L. R. Shang, Y. J. Zhao and Z. Z. Gu, Nanoscale. 2015, 7, 10590.
27 C. H. Alarco´n, S. Pennadam and C. Alexander, Chem. Soc. Rev., 2005, 34, 276.
28 S. W. Choi, J. W. Xie and Y. N. Xia, Adv. Mater., 2009, 21, 2997.
29 A. Stein, B. E. Wilson and S. G. Rudisill, Chem. Soc. Rev. 2013, 42, 2763.
30 W. Hong, H. R. Li, X. B. Hu, B. Y. Zhao, F. Zhang and D. Zhang, Chem. Commun. 2012, 48, 4609.
31 Y. S. Zhang, S. W. Choi, Y. N. Xia, Soft Matter, 2013, 9, 9747.
32 J. W. Hou, Q. Shi, W. Ye, P. Stagnaro, and J. H. Yin, Chem. Commun., 2014, 50, 14975.
33 J. W. Hou, Q. Shi, W. Ye, Q. F. Fan, H. C. Shi, S. C. Wong, X. D. Xu and J. H. Yin, Chem. Commun., 2015,51, 4200.